Statistical mechanics of ionic colloids: Interparticle correlations and conformational equilibria in suspensions of polymer coated colloids

David Ronis
Department of Chemistry, McGill University, 801 Sherbrooke Street West, Montreal, Quebec, Canada H3A 2K6
(Received 21 January 1994)

Ornstein-Zernike integral equations using hybrid closures, developed to study the intra-aggregate correlations in polymer coated colloids, are combined with a mean-field Monte Carlo description of the polymers attached to the aggregates. The equilibrium coupling between the intra-aggregate correlations and conformations of the attached polymers is examined, and results for the aggregate-aggregate pair correlation functions, structure factors, and local monomer densities, for charged and neutral chains, at low and high surface coverage and concentration are presented.

PACS number(s): 82.70.Dd, 61.25.Hq, 05.20.−y

I. INTRODUCTION

Colloidal suspensions can be stabilized either sterically or electrostatically. In electrostatic stabilization, the colloidal particles are charged, and the solvent's ionic strength is kept low so that the resulting Coulomb barrier is large compared to thermal energies. In steric stabilization, polymer chains are attached to the colloidal particle's surface, either through adsorption or chemically, e.g., by forming the colloid as a micelle of block copolymers. The polymer coated aggregates are placed in a good solvent and polymer-polymer repulsion keeps the colloidal cores apart. Of course, both methods can be combined by using polyelectrolyte polymers.

Colloid-polymer interactions have been the subject of much study recently [1]. Experimental approaches have measured dynamic and static scattering, thermodynamic properties, atomic force microscopy, adsorption kinetics, and hydrodynamics to probe the nature of the adsorbed layers. Theoretical approaches usually involve phenomenological scaling arguments or mean-field theories or have relied on computer simulation. In the numerical approaches, the complications associated with charged systems are ignored and the studies are restricted to relatively short, neutral chains. In addition, most theoretical works are restricted to systems at infinite dilution, or to systems where there are one or two fixed, simple surfaces to which the polymers are attached.

Conformal equilibrium in polymeric solutions has been a major area of research. As in the preceding paragraph, theoretical approaches have used all the tools of statistical mechanics: mean-field arguments [2], scaling and renormalization group methods [3], computer simulations [4], and more recently, extensions of integral equation methods used to describe molecular liquids [5]. The latter two approaches should, in principle, allow one to start from a molecular model of the polymer, however, some aspects of the integral equation methods are *ad hoc*, and both involve considerable numerical effort, even for neutral chains.

None of the methods just mentioned deals with the problem of polymers heterogeneously bound to colloidal surfaces that in turn are homogeneously distributed throughout the solution. In order to do so for nondilute suspensions, the interactions governing the equilibrium conformations of the chains must be considered for polymers that are adsorbed to the same or different colloidal cores, and must be dealt with in a manner that takes the translational equilibrium of the aggregates into account. A way of solving this problem is presented in this work.

If the conformational equilibria of the adsorbed polymers could be ignored, and the average monomer distribution assumed, then the equilibrium statistical mechanics of charged or neutral polymer coated colloidal particles can be studied using the integral equation methods developed in Ref. [6]. This approach was based on the hybrid mean-spherical (MSA)–hypernetted-chain (HNC) approximation developed to study surface-charged colloidal suspensions in Ref. [7]. As was shown in Ref. [6], the integral equations can be solved for arbitrary spherically symmetric monomer distributions, and scattering structure factors, counterion distributions, and thermodynamic properties can be calculated.

A mean-field Monte Carlo method was used in Ref. [8] to study conformational equilibria in ionic-polymer coated, infinitely dilute, colloidal suspensions. There, a mean field was constructed in order to describe the interactions between monomers on the same or different chains, as well as their interactions with the counterions. The mean field was a functional of the average monomer density, and this was calculated self-consistently using a variant of the Monte Carlo algorithm [9]. In addition, in order to simplify the calculation, the counterions were described by the Poisson-Boltzmann equation, in the linearized Debye-Huckel approximation.

Thus, the existing approaches to these problems either ignore the conformational equilibria of the polymer chains or the translational equilibria of the aggregates. In this work, these restrictions will be removed; the approaches of Refs. [6] and [8] will be combined, and a theory for the colloid-colloid structure factors, counterion distributions, and polymer conformational equilibria, at finite colloid concentrations, will be formulated and solved for systems comprised of mobile aggregates

with flexible polymer chains. In the next section, the mean-field potential governing the interactions between aggregates will be specified as a functional of the average monomer density surrounding the colloidal cores. In addition, a mean-field potential experienced by a single monomer due to the counterions, the monomers attached to the same colloid core, and those attached to different colloidal particles will be given as a functional of the average monomer density *and* the aggregate-aggregate or aggregate-counterion pair correlation functions.

Section II also contains an extension of the analysis of the hybrid MSA-HNC approximation developed in Ref. [6] in order to allow for the possibility that the aggregates overlap; even so, it will be shown that the problem of determining the aggregate-aggregate correlation functions can be reduced to a one-component problem with an effective potential, without first having to specify the average monomer distributions or the closure used for the aggregate part of the problem. Section II also reviews the mean-field Monte Carlo method.

The theory is applied to neutral and charged chains and the results are presented in Sec. III. For the concentrations and coverages studied, there turns out to be very little overlap of the polymers attached to different colloids; the conformations of the adsorbed polymers are mainly dependent on the intra-aggregate interactions, i.e., between monomers on the same aggregate, and average distributions are not strongly perturbed by the neighboring aggregates. On the other hand, the aggregate-aggregate correlation functions and structure factors turn out to be very sensitive to the conformation of the adsorbed chains. This is to be expected since the interaggregate correlations are strongly dependent on packing considerations or on the presence of large numbers of poorly screened charges. In addition, in the case of charged chains, the counterion distributions can be calculated and are closely related to the monomer distributions through local electroneutrality. Section III also contains some comparisons between the MSA-HNC approximation and the linearized and nonlinear Poisson-Boltzmann equation for some of the infinite dilution cases studied in Ref. [8]; the approximations yield qualitatively similar results, but there are still important quantitative differences. Finally, Sec. IV contains a summary and discussion.

II. THEORY

A. The potentials

As was discussed in the Introduction, mean-field potentials that depend on the conformation of the polymers attached to the individual colloid particles through the average local monomer density, and that describe the intra- and inter-aggregate interactions, must be constructed; here, this is done phenomenologically.

If the interaction potential between two monomers is denoted by $u_{m,m}(r)$, then the corresponding part of the total interaction potential can be written as

$$U_{m,m} \equiv \sum_{\substack{i,j \\ i \neq j}} u_{m,m}(r_{i,j}) = \int d\mathbf{r}\, d\mathbf{r}'\, N_m(\mathbf{r}) N_m(\mathbf{r}') u_{m,m}(|\mathbf{r}-\mathbf{r}'|)\,, \tag{2.1}$$

where $\mathbf{r}_{i,j} \equiv \mathbf{r}_i - \mathbf{r}_j$, i and j label the monomers [10],

$$N_m(\mathbf{r}) \equiv \sum_j \delta(\mathbf{r}-\mathbf{r}_j), \tag{2.2}$$

is the microscopic form of the total monomer density, and $\delta(\mathbf{r})$ is the Dirac δ function. Strictly speaking, the second equality in Eq. (2.2) requires that $u_{m,m}(0)=0$; however, the total interaction potential is only shifted by an unimportant additive constant should this not be the case.

The mean-field potentials are constructed by preaveraging Eq. (2.1) and ignoring monomer-monomer correlations. First consider the monomer-monomer contribution to the colloid-colloid center-of-mass–center-of-mass interaction. This is obtained by replacing the microscopic monomer densities in Eq. (2.1) by averaged ones, specifically, by $\rho_m(\mathbf{r})$, which is the average density of monomers associated with the polymers attached to any specific colloid (whose center is defined to be the origin). Hence, the effective colloid-colloid interaction potential for two colloidal particles at center-of-mass separation $\mathbf{R}_{i,j}$ becomes

$$u_{c,c}(R_{i,j}) = u_{c,c}^{(0)}(R_{i,j}) + \int d\mathbf{r}\, d\mathbf{r}'\, \rho_m(\mathbf{r}+\mathbf{R}_{i,j}) \times u_{m,m}(\mathbf{r}+\mathbf{R}_{i,j}-\mathbf{r}')\rho_m(\mathbf{r}'), \tag{2.3}$$

where $u_{c,c}^{(0)}(r)$ is the potential describing the direct interaction between the colloid cores; in this work, this will be taken as an additive hard-sphere potential. Note that the integrals appearing on the right hand side of Eq. (2.3) are convolutions, and hence, may be evaluated by Fourier transform; this will simplify the numerical work discussed below.

In ionic systems the colloid counterions or any extra salt ions should be considered explicitly [6,7,11]. The interactions between the ions will be described by a primitive electrolyte model, while those between the ions and a colloidal aggregate will be treated within the mean-field approximation used in the last paragraph. Specifically, the interaction potential between an ion of type i at $\mathbf{r}$ and a colloidal aggregate at the origin becomes

$$u_{i,c}(r) = u_{i,c}^{(0)}(r) + \int d\mathbf{r}'\, u_{i,m}(|\mathbf{r}-\mathbf{r}'|)\rho_m(r'), \tag{2.4}$$

where $u_{i,c}^{(0)}(r)$ describes the interaction of the ion and the colloid core and will be modeled by an additive hard-sphere potential. In addition, $u_{i,m}(r)$ describes the interaction between the ion and a monomer and has both electrostatic and nonelectrostatic contributions. Again note that the integral in Eq. (2.4) is a convolution.

Finally, the mean-field experienced by a given monomer must be specified, and this has several components: the interactions with the other monomers attached to the same colloidal core; the interactions with those attached

to different colloids; and lastly, the interactions with the salt ions. In order to specify these, note that the density of ions of type i around a colloidal particle at the origin can be simply expressed in terms of $g_{i,c}(r)$, the i-colloid pair correlation function as

$$\rho_i g_{i,c}(r), \tag{2.5a}$$

where ρ_i is the bulk number density of i. Similarly, if direct monomer-monomer correlations are ignored, then the total density of monomer around a colloid at the origin is

$$\rho_{m,\text{total}}(r) \equiv \rho_m(r) + \rho_c \int d\mathbf{R}\, g_{c,c}(R)\rho_m(|\mathbf{r}-\mathbf{R}|), \tag{2.5b}$$

where $g_{c,c}(r)$ is the colloid-colloid, center-of-mass, pair correlation function and ρ_c is the bulk colloid number density. The first term in Eq. (2.5b) arises from the monomers attached to the colloid at the origin, while the second is due to monomers attached to different colloids.

With the last two expressions for the local densities, an approximate expression for the potential felt by a single monomer attached to a colloid whose center is at the origin is easy to obtain; i.e.,

$$\phi(r) = \phi^{(0)}(r) + \sum_i \int d\mathbf{r}'\, u_{i,m}(|\mathbf{r}-\mathbf{r}'|)\rho_i g_{i,c}(\mathbf{r}') + \int d\mathbf{r}'\, u_{m,m}(|\mathbf{r}-\mathbf{r}'|)\left[\rho_m(r') + \rho_c \int d\mathbf{R}\, g_{c,c}(R)\rho_m(|\mathbf{r}'-\mathbf{R}|)\right], \tag{2.6}$$

where $\phi^{(0)}(r)$ describes the interaction of the monomer and the colloid core and will be taken to be a hard-sphere potential. In addition, there should be a term in Eq. (2.6) due to the interaction of monomers attached to the colloid at the origin with the cores of its neighbors; however, for the models to be studied below, it turns out that the polymer layers never overlap to the extent where this term would be significant.

Analogs of the first three terms on the right-hand side of Eq. (2.6) already appeared in Ref. [8]; the last term is new and arises from the interactions between colloids on different particles. In addition, note that the colloid-counterion interaction depends on $g_{i,c}(r)$, which will depend on the approximations used to describe the electrolyte correlations (in Ref. [8], the linearized Debye-Huckel approximation was used).

Finally, the approximate nature of the potentials presented in this section cannot be overemphasized. One manifestation of this is that some of the integrals will diverge if the underlying potential functions, $u_{m,m}(r)$ or $u_{i,m}(r)$, diverge faster than r^{-3} as $r \to 0$. This reflects the fact that rigorous expansions of the potentials of mean force typically involve the Mayer-f functions or direct correlation functions, and these only become proportional to the underlying potentials when the interactions are weak. Moreover, only the leading-order terms in these expansions will be similar to those presented here, and in part, the higher-order corrections describe the three-body monomer-monomer correlations that have been ignored.

As a result of the approximations introduced above, the effective potentials describing the interactions between the counterions and the colloid-polymer aggregates, $u_{i,c}(r)$ and $u_{c,c}(r)$ are simple functionals of the monomer density; hence, if this is known, then the resulting potentials can be used in a theory similar to that developed in Ref. [6] to compute the correlation functions. Conversely, if the correlation functions were known, then the effective potential felt by a single monomer, $\phi(r)$, is a functional of $\rho_m(r)$, and thus single-chain properties can be computed self-consistently by using the mean-field Monte Carlo method presented in Ref. [8]. Of course, neither the correlations nor the monomer density is really known *a priori*, but as will be shown below, there is a simple way to combine these two approaches and to self-consistently solve the coupled problems. Before turning to this, some modifications to the calculation presented in Ref. [8] must be considered.

B. The correlation functions

For the purpose of the discussion in this subsection, the monomer density, $\rho_m(r)$ is assumed to be known and the correlation functions will be determined using the effective potentials given above, cf. Eqs. (2.3) and (2.4). The starting point of many theories of correlations in condensed systems is the Ornstein-Zernike equation [12]

$$\underline{h} = \underline{c} + \underline{c} \circ \underline{\rho}\, \underline{h}, \tag{2.7}$$

where $\circ$ denotes a convolution, matrices are denoted by underbars, $h_{i,j}(r) \equiv g_{i,j}(r) - 1$, $c_{i,j}(r)$ is the direct correlation function for components i and j, and $\underline{\rho}$ is a diagonal matrix whose entries are the bulk densities of each component.

A closure relating $\underline{c}$ and $\underline{h}$ is required before the correlation functions can be determined. Several have been tried for dilute suspensions of highly charged colloidal or micellar particles. For example, there is the hypernetted-chain approximation (HNC) in which

$$g_{i,j}(r) = e^{-\beta u_{i,j}(r) + h_{i,j}(r) - c_{i,j}(r)}, \tag{2.8}$$

where $\beta \equiv 1/k_B T$. Unfortunately, attempts at solving the resulting system of nonlinear integral equations haven't proved very successful for the range of charges and densities typically found in the colloidal systems. One notable exception is the numerical HNC work of Belloni [13] for moderately charged micellar systems.

An alternative closure is the mean-spherical approximation (MSA) [14]. When the particles have a hard core, this approximation requires that

$$h_{i,j}(r) = -1 \quad \text{for } r \le R_{i,j}, \tag{2.9a}$$

while

$$c_{i,j}(r) = -\beta u_{i,j}(r) \quad \text{for } r > R_{i,j}, \tag{2.9b}$$

where $R_{i,j}$ is the closest approach distance for a pair of

particles of types i and j. The MSA has the advantage that the resulting equations can be solved either exactly, or by solving a small number of algebraic equations, for several potentials; nonetheless, the results are usually poor for the range of charges and densities found in colloidal suspensions; in particular, the correlation functions have their main structural features at the wrong length scales [11].

In Ref. [7] it was recognized that part of the problem with the MSA is its inability to correctly describe the effects of a strongly repulsive interaction that has a characteristic length that is much different than the core size; this is not the case with the HNC. Moreover, since it was known that the MSA fortuitously gives a better description of electrode double layers than the HNC, a hybrid closure was proposed; namely, the MSA was used for all correlation functions that refer to the counterions, while HNC was used for the colloid-colloid correlation functions.

Another aspect of the work of Refs. [6,7,11] showed that if the counterion radius was set to zero, then the parts of the problem explicitly referring to these components could be analytically eliminated from the problem, resulting in a problem where the remaining colloid components interact via a screened Coulomb interaction with an effective charge that depends on the colloid-colloid correlations and that must be determined self-consistently.

In Ref. [6], the hybrid closure approach was extended to models where the colloids were surrounded by a specified, extended charge region (e.g., as would be the case when charged polymer chains are attached to the colloid core). For the purpose of the calculation in Ref. [6] it was assumed that colloid-colloid closest approach distances were chosen so that the charged regions corresponding to different colloidal particles couldn't overlap. In this work, the only fixed size for the colloidal particles is the inner core radius; the polymers are flexible, and the results of Ref. [6], cannot be applied without modification.

The initial steps of the derivation are the same as in Ref. [6]. The counterions are assumed to have zero radius, charge z_i, and interact solely via Coulomb's law:

$$u_{i,j}(r)=\frac{z_i z_j}{\epsilon r}, \tag{2.10}$$

where ϵ is the dielectric constant of the solvent (recall that the primitive model is assumed, and hence, the solvent is not considered explicitly). Since the counterion parts of the problem were assumed to satisfy the MSA, the system of equations can be transformed so that only a single charged effective counterion component is present. Specifically, the point-ion blocks of the density scaled correlation functions, $H_{i,j}(r)\equiv(\rho_i\rho_j)^{1/2}h_{i,j}(r)$ and $C_{i,j}(r)\equiv(\rho_i\rho_j)^{1/2}c_{i,j}(r)$, are transformed with an orthogonal transformation, $\underline{P}$; i.e., $\underline{H}'\equiv\underline{P}^T\underline{H}\,\underline{P}$ and $\underline{C}'\equiv\underline{P}^T\underline{C}\,\underline{P}$. The transformation matrix $\underline{P}$ is block diagonal with a unit colloid-colloid block, while the matrix elements of the point-ion block are given by

$$P_{i,j}\equiv\frac{\delta_{j,1}z_i\sqrt{\rho_i}}{I^{1/2}}+(1-\delta_{j,1})\left[\delta_{i,j}-\frac{z_j\sqrt{\rho_j}(\delta_{i,1}I^{1/2}+z_i\sqrt{\rho_i})}{I^{1/2}(I^{1/2}+z_1\sqrt{\rho_1})}\right], \tag{2.11a}$$

where

$$I\equiv\sum_{i=1}\rho_i z_i^2 \tag{2.11b}$$

is the ionic strength of the point ions [15]. Henceforth, 1 will refer to the counterions of the colloid component and 2,... to the ions of the added salt. Note that electroneutrality requires that

$$z_1\rho_1+\rho_c z_c=0 \tag{2.12a}$$

and

$$\sum_{i=2}\rho_i z_i=0, \tag{2.12b}$$

where z_c is the total charge bound to a colloid particle [16].

When the transformation is carried out, the forms of the Ornstein-Zernike equations and MSA closures for the point ions are preserved. Some simple algebra shows that $z_i\rightarrow z_p\delta_{i,1}$, where

$$z_p\equiv\frac{I}{z_1\rho_1}, \tag{2.13a}$$

and $\rho_i\rightarrow\rho_i'$, where

$$\rho_i'\equiv\left[\sum_{j=1}^{m}P_{j,i}\sqrt{\rho_j}\right]^2=\begin{cases}\rho_p\equiv(z_1\rho_1)^2I^{-1} & \text{for } i=1\\ \rho_i I^{-1}(I^{1/2}-z_i\rho_1^{1/2})^2 & \text{for } i=2,\ldots\ .\end{cases} \tag{2.13b}$$

The effective densities were obtained by examining the colloid–point-ion core conditions. Note that electroneutrality still holds; i.e.,

$$z_p\rho_p+\rho_c z_c=0. \tag{2.14}$$

Thus, in the transformed representation, there is only a single charged counterion; the other counterions are neutral, and since they have zero diameter, their correlation functions are trivially obtained (see below). Finally, note that the electrostatic parts of the effective potentials given in Eqs. (2.3), (2.4), and (2.6) also transform as expected; the neutral components drop out while the charge and density for component 1 become the effective charge z_p and effective density ρ_p, respectively.

Henceforth, only the transformed correlation functions will be considered and the primes will be dropped. The only nonvanishing direct correlation functions for the

neutral components, denoted by n, is $c_{n,c}(r)$ for $r<R_{n,c}$, and, as long as $R_{c,c}\geq 2R_{n,c}$, the same result as found in the earlier works [6,11,7] is obtained by examining the $n-c$ component of the Ornstein-Zernike equations for $r\leq R_{n,p}$; specifically,

$$c_{n,c}(r)=\frac{1}{\xi_{p,c}-1}, \tag{2.15}$$

where

$$\xi_{p,c}\equiv\tfrac{4}{3}\pi R_{n,c}^3\rho_c \tag{2.16}$$

is the $p-c$ packing fraction. Similarly, it is easy to see from the Ornstein-Zernike equations for the colloid-colloid and neutral-colloid correlation functions that the neutral components can be ignored as long as the colloid-colloid direct correlation function is replaced by

$$c_{c,c}(r)+\sum_n c_{c,n}\rho_n\circ c_{c,n} \tag{2.17}$$

in the equations describing the non-neutral species. Moreover, since the convolution terms vanish for $r\geq 2R_{n,c}$ and $R_{c,c}\geq 2R_{n,c}$, this modification will have no effect on the HNC closure outside the $c-c$ closest approach distance, and can be ignored for the purposes of calculating the correlation functions [17].

If the remaining p and c components of the Ornstein-Zernike equations are Fourier transformed in space, they can easily be rearranged to show that $h_{c,c}(r)$ obeys an effective single-component equation of the form

$$h_{c,c}(r)=c_{c,c}^{(1)}(r)+c_{c,c}^{(1)}\circ\rho_c h_{c,c}, \tag{2.18}$$

where

$$\tilde{c}_{c,c}^{(1)}(k)\equiv\tilde{c}_{c,c}(k)+\frac{\rho_p k^2\tilde{c}_{c,p}^2(k)}{k^2+\kappa_D^2}, \tag{2.19}$$

where tildes henceforth denote spatial Fourier transforms, k is the Fourier transform wave vector, and

$$\kappa_D\equiv\sqrt{4\pi\beta I/\epsilon} \tag{2.20}$$

is the inverse Debye screening length. Note that as long as the closure for the colloid-colloid correlations in the multicomponent problem can be written as a functional of the form $h_{c,c}(r)=F(r|h_{c,c}(r'),\beta u_{c,c}(r')+c_{c,c}(r'))$, then the effective one-component equation can be viewed as obeying the same closure, but with an effective potential, $u_{c,c}^{(1)}(r)$; specifically, in its Fourier representation,

$$\tilde{u}_{c,c}^{(1)}(k)\equiv\tilde{u}_{c,c}(k)-\frac{\rho_p k^2\tilde{c}_{c,p}^2(k)}{k^2+\kappa_D^2}. \tag{2.21}$$

The other correlations can easily be expressed in terms of $\tilde{c}_{p,c}(k)$ and $\tilde{h}_{c,c}(k)$; specifically,

$$\tilde{h}_{p,p}(k)=\frac{-4\pi\beta z_p^2/\epsilon+k^2\tilde{c}_{p,c}(k)\rho_c\tilde{h}_{c,c}(k)}{k^2+\kappa_D^2} \tag{2.22a}$$

and

$$\tilde{h}_{p,c}(k)=\frac{k^2\tilde{c}_{p,c}(k)[1+\rho_c\tilde{h}_{c,c}(k)]}{k^2+\kappa_D^2}. \tag{2.22b}$$

In order to determine the form $c_{p,c}(r)$ for $r\leq R_{p,c}$ consider the $p-c$ component of the Ornstein-Zernike equations in bispherical coordinates and use the MSA closure given in Eq. (2.9). This shows that

$$c_{p,c}(r)=B+\frac{2\pi\rho_c}{r}\int_{R_{p,c}}^{\infty}d\eta\,\eta\beta\Delta u_{p,c}(\eta)\int_{\eta-r}^{\eta+r}d\xi\,\xi h_{c,c}(\xi) \tag{2.23a}$$

$$=\Gamma_{p,c}+\frac{2\pi\rho_c}{r}\int_{R_{c,c}-R_{p,c}}^{\infty}d\eta\,\eta\beta\Delta u_{p,c}(\eta)\int_{\eta-r}^{\eta+r}d\xi\,\xi h_{c,c}(\xi), \tag{2.23b}$$

for $r<R_{p,c}$, where

$$B\equiv-1-\kappa_D^2\left[\int_0^{\infty}dr\,r\,[h_{c,c}(r)-h_{p,c}(r)]+\tfrac{1}{2}R_{p,c}^2\right]+4\pi\rho_c\int_0^{R_{p,c}}dr\,r^2c_{p,c}(r), \tag{2.24a}$$

$$u_{p,c}(r)\equiv\Delta u_{p,c}(r)+\frac{z_c z_p}{\epsilon r}, \tag{2.24b}$$

and

$$\Gamma_{p,c}\equiv B+4\pi\rho_c\int_{R_{p,c}}^{R_{c,c}-R_{p,c}}dr\,r^2\beta\Delta u_{p,c}(r). \tag{2.24c}$$

In Ref. [6], it was assumed that the polymeric regions do not overlap, and thus, $\Delta u_{p,c}(r)=0$ for $r>R_{c,c}-R_{p,c}$. In such cases, the last term on the right-hand side of Eq. (2.23b) vanishes and $c_{p,c}(r)=\Gamma_{p,c}$ is constant within the core. In this work, the no-overlap assumption must be relaxed [18]. Nonetheless, it is still possible to determine the constant B in terms of integrals of $h_{c,c}(r)$ and the potentials.

By multiplying Eq. (2.23a) by $4\pi\rho_c r^2$ and integrating from 0 to $R_{p,c}$ it follows that

$$B=\frac{\kappa_D^2\left[\int_0^{\infty}dr\,r[h_{p,c}(r)-h_{c,c}(r)]-\frac{1}{2}R_{p,c}^2\right]-1+A}{1-\xi_{p,c}}, \tag{2.25}$$

where

$$A \equiv 8\pi^2\rho_c^2 \int_0^{R_{p,c}} dr\, r \int_{R_{p,c}}^{\infty} d\eta\, \eta\beta\Delta u_{p,c}(\eta) \times \int_{\eta-r}^{\eta+r} d\xi\, \xi h_{c,c}(\xi). \tag{2.26}$$

In order to determine B, and hence $c_{p,c}(r)$, in terms of $h_{c,c}(r)$ or known functions, note the following identity:

$$\hat{f}(s) \equiv \int_0^{\infty} dr\, re^{-sr} f(r) = \int_0^{\infty} \frac{dk}{2\pi^2} \frac{k^2 \tilde{f}(k)}{s^2+k^2}. \tag{2.27}$$

If this last result is applied to the integral in Eq. (2.25), it follows that

$$\int_0^{\infty} dr\, r[h_{p,c}(r)-h_{c,c}(r)] = \lim_{s\to 0+} \int_0^{\infty} \frac{dk}{2\pi^2} \frac{k^2}{s^2+k^2} \left\{ \frac{k^2 \tilde{c}_{p,c}(k)[1+\rho_c \tilde{h}_{c,c}(k)]}{k^2+\kappa_D^2} - \tilde{h}_{c,c}(k) \right\}, \tag{2.28}$$

where Eq. (2.22b) was used for $\tilde{h}_{p,c}(k)$. It is easy to show that the quantity in the curly brackets in Eq. (2.28) is analytic at $k=0$ and that the $s\to 0+$ limit can be taken inside the integration.

The B dependence in Eq. (2.28) can be made explicit by using Eq. (2.23a), specifically, by writing

$$\tilde{c}_{p,c}(k) = B 4\pi R_{p,c}^3 j_1(kR_{p,c})/kR_{p,c} + D(k), \tag{2.29}$$

where $j_1(x) \equiv [\sin(x) - x\cos(x)]/x^2$ is a spherical Bessel function and where

$$D(k) \equiv -\frac{4\pi\beta z_p z_c \cos(kR_{p,c})}{\epsilon k^2} + \frac{8\pi^2\rho_c}{k} \int_0^{R_{p,c}} dr \sin(kr) \int_{R_{p,c}}^{\infty} d\eta\, \eta\beta\Delta u_{p,c}(\eta) \int_{\eta-r}^{\eta+r} d\xi\, \xi h_{c,c}(\xi) - \frac{4\pi}{k} \int_{R_{p,c}}^{\infty} dr\, r\sin(kr)\beta\Delta u_{p,c}(r). \tag{2.30}$$

Finally, Eqs. (2.28)–(2.30) can be used in (2.25) resulting in a linear equation for B that when solved gives

$$B = \frac{\kappa_D^2 \left[\int_0^{\infty} \frac{dk}{2\pi^2} \left[\frac{k^2 D(k)[1+\rho_c \tilde{h}_{c,c}(k)]}{k^2+\kappa_D^2} - \tilde{h}_{c,c}(k) \right] - \frac{1}{2} R_{p,c}^2 \right] - 1 + A}{1 - \xi_{p,c} - \frac{2(\kappa_D R_{p,c})^2}{\pi} \int_0^{\infty} dk \frac{k j_1(kR_{p,c})[1+\rho_c \tilde{h}_{c,c}(k)]}{k^2+\kappa_D^2}}. \tag{2.31}$$

An alternate expression for B can be found directly from the core condition for $h_{p,c}(r)$ at $r=0$ [Eq. (2.9a)], together with Eq. (2.22b); hence,

$$-1 = \int_0^{\infty} \frac{dk}{2\pi^2} \frac{k^4 \tilde{c}_{p,c}(k)[1+\rho_c \tilde{h}_{c,c}(k)]}{k^2+\kappa_D^2}. \tag{2.32}$$

When Eq. (2.29) is used for $\tilde{c}_{p,c}(k)$ in the last expression, it follows that

$$B = -\frac{2\pi^2 + \int_0^{\infty} dk \frac{k^4 D(k)[1+\rho_c \tilde{h}_{c,c}(k)]}{k^2+\kappa_D^2}}{4\pi R_{p,c}^2 \int_0^{\infty} dk \frac{k^3 j_1(kR_{p,c})[1+\rho_c \tilde{h}_{c,c}(k)]}{k^2+\kappa_D^2}}. \tag{2.33}$$

Thus, B has been expressed in terms of integrals, the $p-c$ potential, and $h_{c,c}(r)$, using either of Eqs. (2.31) or (2.33). Once B is computed, $c_{p,c}(r)$ is known and it is a simple matter to evaluate the remaining counterion correlations, cf. Eqs. (2.22a) and (2.22b). Moreover, the effective one-component potential governing the remaining $c-c$ correlations becomes a simple functional of $h_{c,c}(r)$, and this may be determined self-consistently using the method of Refs. [6,7]. Of course, the integrals in Eq. (2.31) must still be evaluated, but a discussion of this point is deferred until Sec. III.

C. Mean-field Monte Carlo

The potentials used in the preceding subsection depend on the average monomer density surrounding a colloid core, cf. Eqs. (2.3) and (2.4). In turn, the average monomer density appears in the mean-field potential acting on the monomers, cf. Eq. (2.6), and this must be determined self-consistently. The mean-field Monte Carlo method introduced in Ref. [8] will be used to accomplish this, and the method will now be summarized.

The mean-field Monte Carlo method follows the original Metropolis [9] scheme in most respects. The configurations of a single polymer chain in an external field are sampled subject to the constraints imposed by the chain's connectivity and by the fact that one end is attached to an impenetrable colloid core. The total potential energy, E_n, of the nth configuration is computed using the effective monomer potential, $\phi(r)$, given in Eq. (2.6), and the configuration is accepted with probability P, where

$$P \equiv \begin{cases} 1 & \text{if } E_n \le E_{n-1} \\ e^{-\beta(E_n - E_{n-1})} & \text{if } E_n > E_{n-1}. \end{cases} \tag{2.34}$$

The resulting Markov chain of configurations can be

used to compute any single-chain property, and in particular, the average monomer density can be computed in this manner [19]. The only difference between the standard Monte Carlo method and mean-field Monte Carlo comes from the need to update the effective monomer potential, $\phi(r)$, using the average monomer density computed after a specified number of Monte Carlo steps. The entire process is repeated until convergence is obtained. As was remarked in Ref. [8], the effective monomer potentials turn out to be relatively smooth and converge rapidly.

As in Ref. [8], the polymer backbone will be modeled as a freely jointed chain of fixed bonds, each of length a. Configurations will be sampled using the *displacement method* in which a single bond is randomly displaced, keeping the bond length fixed. The bond orientations are specified by θ and ϕ, the bond's polar and azimuthal angles, respectively, and these are changed through the following relations:

$$\cos(\theta_{\text{new}})=f(\cos(\theta_{\text{old}})+1+\gamma_\theta\xi;2)-1 \tag{2.35}$$

and

$$\phi_{\text{new}}=f(\phi_{\text{old}}+\gamma_\phi\xi;2\pi), \tag{2.36}$$

where $\xi\in[-\frac{1}{2},\frac{1}{2}]$ is a uniformly generated random number,

$$f(x;y)\equiv\begin{cases}x+y & \text{for } x<0\\ x-y & \text{for } x>y\\ x & \text{otherwise}\end{cases} \tag{2.37}$$

and where $\gamma_{\theta(\phi)}\leq 1$ is used to adjust the size of the step in $\theta(\phi)$.

III. SOME NUMERICAL CONSIDERATIONS AND RESULTS

The methods described in the preceding section will be combined by solving the HNC-MSA equations every time the effective monomer potential, $\phi(r)$, is updated. At each update point in the Monte Carlo run, the current average monomer density is computed, the colloid-colloid and colloid-counterion potentials [cf. Eqs. (2.3) and (2.4)] are evaluated, and the HNC-MSA equations are solved using a Picard iteration scheme with Broyles mixing in which the effective one-component colloid-colloid potential [cf. Eq. (2.21)] is updated at each iteration. In actual practice, the HNC-MSA equations are not iterated until convergence is obtained since the underlying average monomer density, $\rho_m(r)$ is very inaccurate during the initial portions of the Monte Carlo run. Moreover, $\rho_m(r)$ is very jagged initially, and this makes it difficult to attain convergence in the initial Picard iterations. Finally, for the results to be presented below, the parameter B, cf. Eqs. (2.23a) and (2.25), will be computed using Eq. (2.31).

For the results to be presented below, the colloids were assumed to have an impenetrable core of radius $R_0=R_{p,c}=\frac{1}{2}R_{c,c}$. In addition, the counterion-monomer interaction is assumed to be purely electrostatic, i.e., $u_{m,i}(r)=z_iz_m/\epsilon r$, while the monomer-monomer interaction has electrostatic and Flory excluded volume [2] parts, specifically,

$$u_{m,m}(r)\equiv\frac{z_m^2}{\epsilon r}+k_BT\nu\delta(\mathbf{r}), \tag{3.1}$$

where ν is a phenomenological parameter typical of the volume excluded by a single monomer.

In solving the coupled HNC-MSA equations, the Ornstein-Zernike equations are solved by Fourier transforms which are computed by using the fast Fourier transform algorithm. Similarly, the potentials [cf. Eqs. (2.3), (2.4), and (2.6)] and $D(k)$ [cf. Eq. (2.30)] involve multiple convolution integrals that can be also computed using Fourier transforms. For example, consider $\Delta\phi(r)\equiv\phi(r)-\phi^{(0)}(r)$, the part of the effective monomer potential outside the core. From Eq. (2.6) it follows that

$$\Delta\tilde{\phi}(k)=\tilde{u}_{p,m}(k)\rho_p\tilde{h}_{p,c}(k)+\tilde{u}_{m,m}(k)\tilde{\rho}_m(k)[1+\rho_c\tilde{h}_{c,c}(k)] \tag{3.2a}$$

$$=\left[\frac{k^2\tilde{c}_{p,c}(k)\rho_p\tilde{u}_{p,m}(k)}{k^2+\kappa_D^2}+\tilde{u}_{m,m}(k)\tilde{\rho}_m(k)\right]\times[1+\rho_c\tilde{h}_{c,c}(k)], \tag{3.2b}$$

where g's have been replaced by h's thereby changing the effective monomer potential by an unimportant additive constant, and where Eq. (2.22b) was used for $\tilde{h}_{p,c}(k)$.

In order to compare this last expression for the effective monomer potential with that based on the linearized Debye-Huckel approximation presented in Ref. [8], $\tilde{c}_{p,c}(k)$ is rewritten as

$$\tilde{c}_{p,c}(k)\equiv-\frac{4\pi\beta z_pz_m\tilde{\rho}_m(k)}{\epsilon k^2}+\tilde{c}^s_{p,c}(k), \tag{3.3}$$

where Eq. (2.4) was used to make the part arising from regions outside the core explicit. When Eqs. (3.1) and (3.3) are used in (3.2b) it follows that

$$\Delta\tilde{\phi}(k)=\left[\left[\frac{4\pi z_m^2}{\epsilon(k^2+\kappa_D^2)}+k_BT\nu\right]\tilde{\rho}_m(k)+\frac{4\pi z_mz_p\rho_p\tilde{c}^s_{p,c}(k)}{\epsilon(k^2+\kappa_D^2)}\right][1+\rho_c\tilde{h}_{c,c}(k)]. \tag{3.4}$$

The effective monomer potential given by Eq. (3.4) differs from that used in Ref. [8] in several ways. First, the factor of $[1+\rho_c\tilde{h}_{c,c}(k)]$ and the term involving $\tilde{c}^s_{p,c}(k)$ drop out at infinite colloid dilution, and hence, describe interaggregate interactions. The term in $\tilde{c}^s_{p,c}(k)$ also drops out for uncharged aggregates. Of the remaining terms, the one involving the excluded volume parameter, ν, is identical to what is found in Ref. [8]. Finally, when the infinite dilution contribution to $\Delta\phi(r)$ due to first term in the parenthesis is expressed in the coordinate representation, it follows that

$$\lim_{\rho_c \to 0} \Delta\phi(r) = k_B T \nu \rho_m(r) + \frac{2\pi z_m^2}{\epsilon r \kappa_D} \int_{R_0}^{\infty} dr'\, r' \rho_m(r') \times \left[e^{-\kappa_D |r-r'|} - e^{-\kappa_D (r+r')} \right]. \tag{3.5}$$

The last term in the square brackets in the integral differs from what was obtained in Ref. [8]. It is easy to see that the difference comes from the imposition of Neumann boundary conditions on the solutions of the Poisson-Boltzmann equation. This boundary condition is obtained from the usual dielectric boundary conditions when they are used in systems with spherically symmetric charge distributions and charge-free cores. The boundary conditions describe the interaction of the charges in the system with their images in the colloid core; these interactions have been omitted from the microscopic potentials, and hence, the lack of agreement is not surprising. Nonetheless, the expressions will agree when $\kappa_D R_0 \to 0$ [cf. Ref. [8] or Eq. (3.7), below].

The first set of results examines two of the cases considered in Ref. [8] (the values of the model parameters for these cases are summarized in Table I). Figures 1–4 show the effects of increasing the colloid concentration on the structure factors [$S_{c,c}(k) \equiv 1 + \rho_c \tilde{h}_{c,c}(k)$] and pair correlation functions, $g_{c,c}(r)$, in an aqueous suspension containing a 1:1 electrolyte whose concentration has been adjusted to give a Debye screening length of 10 Å in the absence of colloid. Remember that the ionic strength includes the counterions of the colloidal particles, and increases significantly over the concentration ranges shown. The dashed curves in Figs. 1–4 show results for the highest colloid concentrations when the counterion concentration has been reduced so as to give an screening length of 10 Å.

As expected, increasing the colloid concentration leads to an increase in the short-range order and a decrease in the osmotic compressibility. Similarly, increasing the repulsive interactions between the colloids, either by increasing the length of the attached polymers or by increasing the screening length, pushes the nearest neighbors to larger radii and leads to an increase of short-range correlations. These trends are similar to what is observed in small-molecule, electrolyte solutions.

At least one aspect of the results shown in Figs. 1–4 differs from what is typically seen. As the colloid concentration is increased, $S_{c,c}(0)$ approaches zero and ultimately can become negative, indicating mechanical instability or a breakdown of the theory. In addition, while the first peak in $S_{c,c}(q)$ grows, the increase is much less than what is observed in small molecule systems, or in surface-charged colloids. Indeed, the so-called Verlet [20] condition, which signals the onset of freezing, is never reached.

The average conformations of the polymer chains and of the adjacent counterions are examined in Figs. 5–14. The total monomer charge (number) density and counterion charge density is shown in Figs. 5–8. The behavior near the colloid core surface is depicted in Figs. 5 and 6; the monomer density shows very little change for the range of densities studied. The monomer density exhibits a characteristic sawtooth form associated with a highly stretched chain (remember that the individual bonds have fixed length). As was the case in Ref. [8], some of the monomers are pushed to shorter radii when the excluded volume interaction is present; hence, the monomer peaks in Fig. 6 are smaller and broader than those in Fig. 5 near the colloid core.

The total monomer density arising from the chains attached to the colloid core centered at the origin and those attached to neighboring chains, $\rho_{m,\text{total}}(r)$ [cf. Eq. (2.5b)], are shown in Figs. 7 and 8. As the data show, increasing the colloid concentration leads to a slight shrinking of the polymer layer. However, this effect is not due to compression of the polymer layers by the neighboring colloids; instead, it is entirely due to the decrease in the screening length associated with the counterions of the colloidal aggregates. Specifically, if the screening length is kept fixed (dashed curves) the monomer density profile for the monomers attached to the colloid is the same as that at infinite dilution. The insets in Figs. 7 and 8 show

TABLE I. Model parameters in water at 298 K ($\epsilon = 78.54$).

Case	R_0 (Å)	N_A	N_m	z_m (e)	a (Å)	$\frac{3\nu}{4\pi a^3}$
(a)	50	100	120	1	5	0
(b)	50	1000	120	1	5	1
(c)	54	87	600	0	2.5	0–5

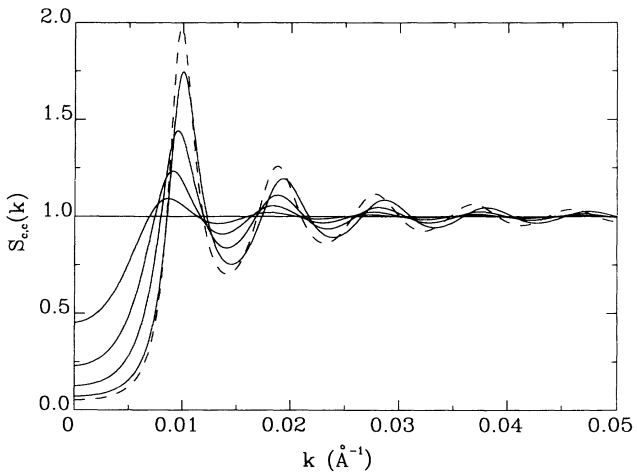

FIG. 1. The density dependence of the colloid-colloid structure factor for a low surface coverage, ionic polymer coated system [case (a) in Table I] in the presence of 1:1 added electrolyte. Results for fixed amounts of added electrolyte ($\lambda_D = 10$ Å at infinite dilution) for colloid concentrations of 0, 1, 2, 3, and 4 μM are shown (solid lines). Also shown is the result when the added electrolyte concentration is adjusted to give a 10 Å screening length (dashed) in the 4 μM suspension. In all cases, monovalent polymer monomer and counterion have been assumed.

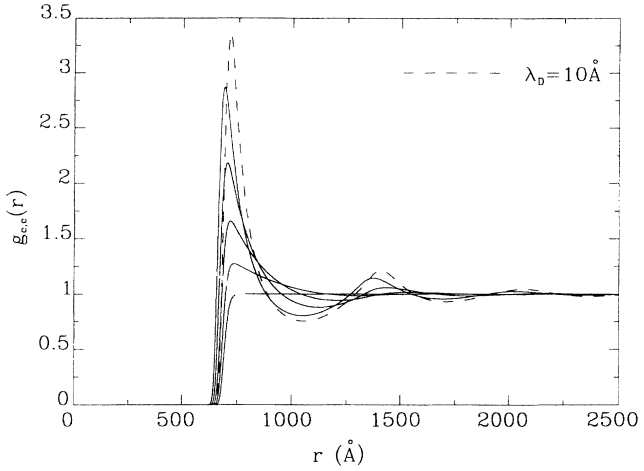

FIG. 2. The density dependence of the colloid-colloid pair correlation function corresponding to the cases shown in Fig. 1.

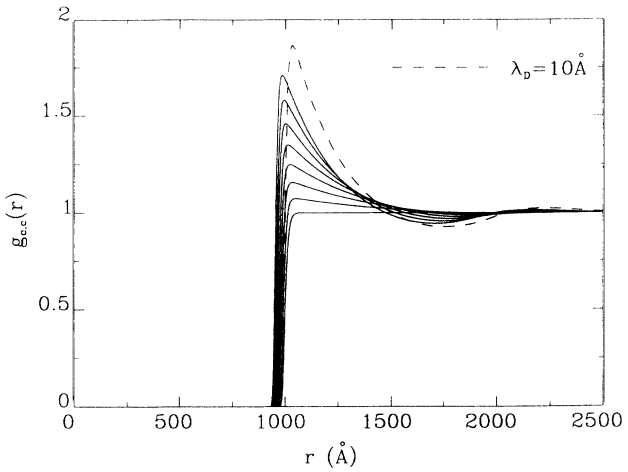

FIG. 4. The density dependence of the colloid-colloid pair correlation function for the densities shown in Fig. 3.

the density of monomers attached to neighboring colloids. While the number of neighboring monomers increases with density, there is no significant interpenetration of the charged polymers associated with different aggregates. The conformations of the bound polymers are governed by the mean-field potential $\phi(r)$, examples of which are shown in Figs. 9 and 10.

The reason why there is so little interpenetrability is apparent from the effective colloid-colloid one-body potentials, $u_{c,c}^{(1)}(r)$, shown in Figs. 11 and 12. As the polymer layers overlap, there is a rapid rise in the effective interaction energy; other aggregates, and hence, their at-

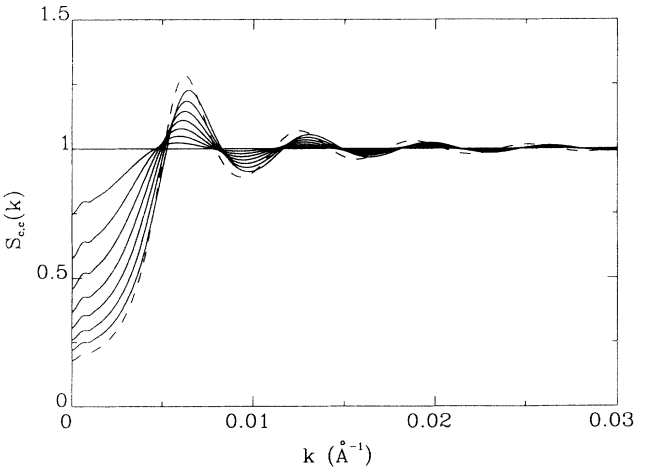

FIG. 3. The density dependence of the colloid-colloid structure factor for a high surface coverage, ionic polymer coated system [case (b) in Table I] in the presence of 1:1 added electrolyte. Results for fixed amounts of added electrolyte ($\lambda_D = 10$ Å at infinite dilution) for colloid concentrations of 0, 0.1, 0.2, . . . , and 0.7 μM are shown (solid lines). The dashed curve was obtained by adjusting the added electrolyte concentration to give a 10 Å screening length in a 0.7 μM suspension. As in Fig. 1, monovalent polymer monomers and counterions have been assumed. The small bumps at small wave vectors are numerical artifacts.

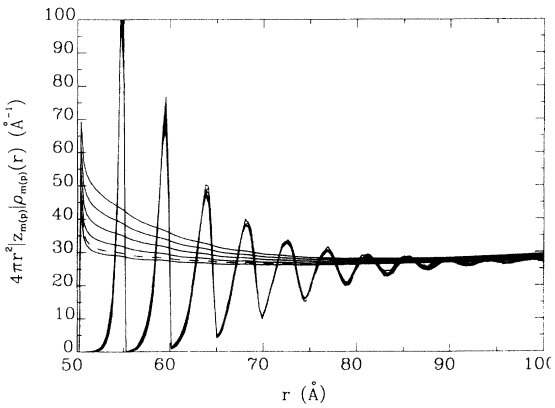

FIG. 5. Total monomer and counterion charge densities near the core surface for the low coverage cases shown in Fig. 1.

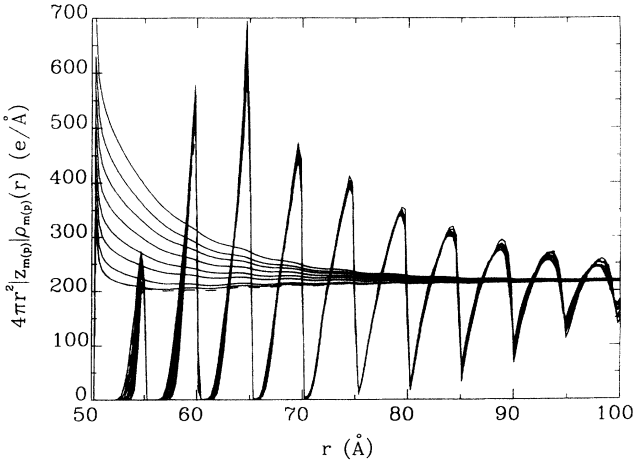

FIG. 6. Total monomer and counterion charge densities near the core surface for the high coverage cases shown in Fig. 2.

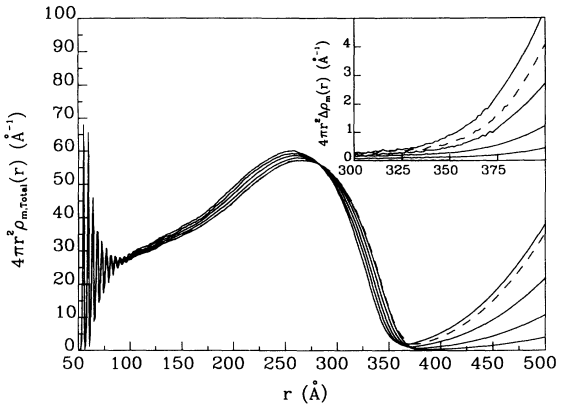

FIG. 7. Total monomer density for the low coverage case shown in Fig. 1. The inset shows the difference between the total monomer density and the part that arises from the polymers attached to the colloid (at r=0).

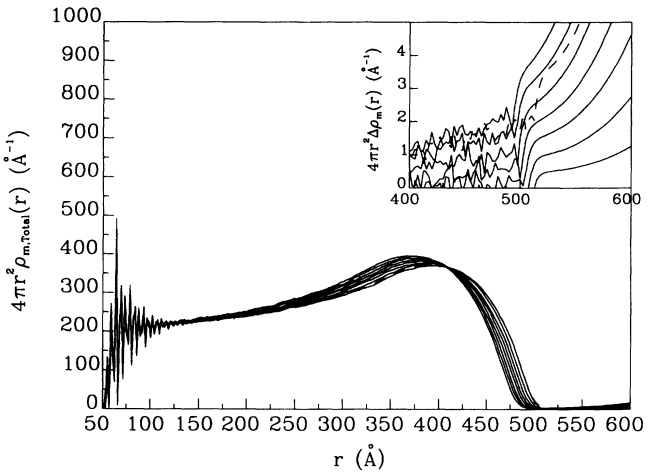

FIG. 8. As in Fig. 7, but for the high coverage cases.

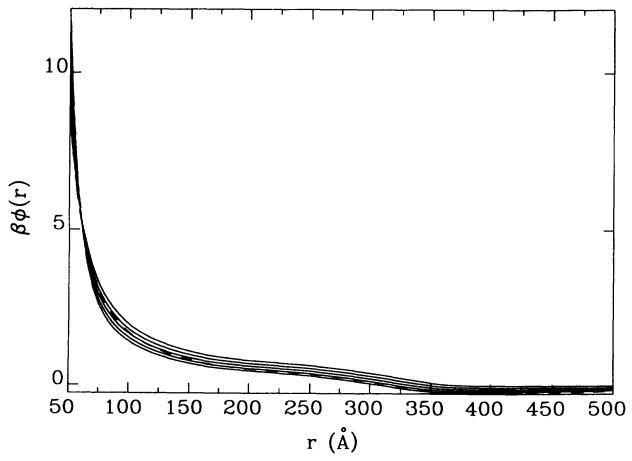

FIG. 9. The monomer mean-field potential, $\phi(r)$ for the low coverage cases, cf. Eqs. (2.6) and (3.2). Remember that $\phi(r)$ is defined only up to an arbitrary additive constant.

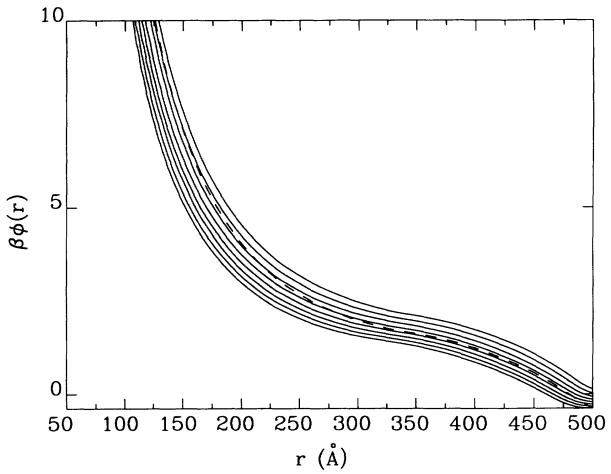

FIG. 10. As in Fig. 9, but for the high coverage cases.

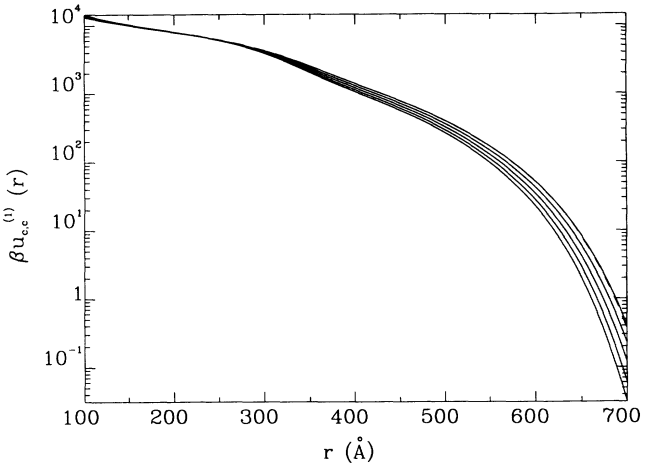

FIG. 11. Effective one-component potentials, cf. Eq. (2.21), for the low coverage cases.

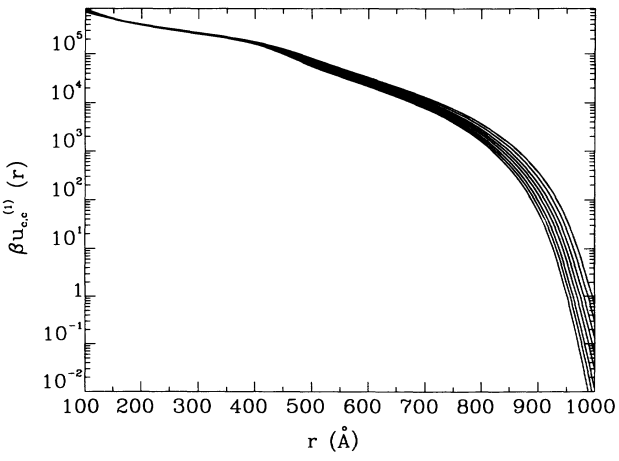

FIG. 12. As in Fig. 11, but for the high coverage cases.

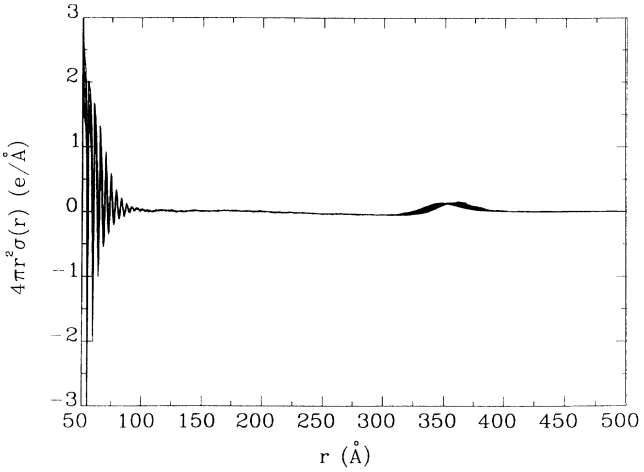

FIG. 13. Total charge density for the low coverage cases.

tached polymers, will be excluded from regions where $u_{c,c}^{(1)}(r) \gg k_B T$. The reason for this rapid increase will be further discussed below.

As is shown in Figs. 5 and 6, the counterions neutralize the monomer charges on a length scale that is comparable to the screening length. The net charge density, $\sigma(r) \equiv z_m \rho_{m,\text{total}}(r) + z_p \rho_p g_{p,c}(r)$ is shown in Figs. 13 and 14. The data show that the polymer charge is locally neutralized except in the highly ordered layers near the core surface and at the outer edge of the aggregate (which is slightly ionized).

Before turning to results for neutral chains, the monomer distributions, at infinite colloid dilution, for several Debye screening lengths are compared with those obtained using the linearized Debye-Huckel approximation. As was pointed out in Ref. [8], under some conditions, the effective potentials can be very large and the validity of the linearized Debye-Huckel approximation is questionable. A third approximation would be to compute the effective monomer potential using the mean electric potential, $\Phi(r)$, obtained from the full nonlinear Poisson-Boltzmann equation; i.e.,

$$\nabla^2 \Phi(r) = -\frac{4\pi}{\epsilon}\{z_m \rho_m(r) - 2 z_s \rho_s \sinh[\beta z_s \Phi(r)]\}, \tag{3.6}$$

where a symmetric $z_s{:}z_s$ electrolyte, with $z_s = e$, has been assumed. In addition, dielectric boundary conditions must be imposed on the solutions to Eq. (3.6), and, as was pointed out above, these imply Neumann boundary conditions at $r = R_0$ for the system under consideration.

In order to solve Eq. (3.6) during the Monte Carlo run, it is first converted to an integral equation by using the Green's function for the linearized equation [cf. Eq. (2.9) of Ref. [8]], thus

$$\Phi(r) = \frac{2\pi}{\kappa_D \epsilon r}\int_{R_0}^{\infty} dr' \left[e^{-\kappa_D |r-r'|} + \frac{(\kappa_D R_0 - 1)}{(\kappa_D R_0 + 1)} e^{-\kappa_D (r + r' - 2R_0)} \right] r' (z_m \rho_m(r') - 2 z_s \rho_s \{\sinh[\beta z_s \Phi(r')] - \beta z_s \phi(r')\}). \tag{3.7}$$

Note that Green's function satisfies the boundary condition at $r = R_0$, and this leads to the difference between the second term in the square brackets and the corresponding term in Eq. (3.5). Equation (3.7) is solved iteratively during the Monte Carlo run, and some results are shown in Figs. 15 and 16.

When the Coulombic interactions are reasonably well screened, cf. Fig. 15, the features of the monomer densities in the three approaches are qualitatively similar; i.e., the overall dimensions of the chains are comparable and the extent of strongly stretched chain. One significant difference is the absence in the HNC-MSA results of the sudden rise in the monomer density seen in both Poisson-Boltzmann equation-based theories. As was discussed in Ref. [8], this rise is associated with a sudden melting of the ionic chain (it is highly stretched and rodlike closer to the core), but may be an artifact of the approximation. This is perhaps not surprising, since the electrolyte solution needed to give a 10 Å screening length is not dilute, and hence, there is no good reason to expect that a Poisson-Boltzmann description of the electrolyte will be sufficient.

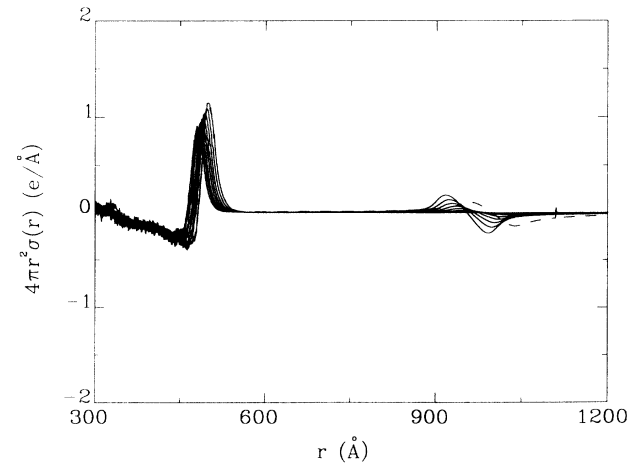

FIG. 14. Total charge density for the high coverage cases.

Figure 16 shows results for much more dilute electrolyte solutions. Here the results using the HNC-MSA and linearized Debye-Huckel approximations are almost identical, as expected from the discussion after Eq. (3.5); the figures show a highly stretched chain. On the other hand, the nonlinear Poisson-Boltzmann equation results are qualitatively different, in that the polyelectrolyte is much less swollen, and the extent of the highly stretched rodlike region is much smaller (this last aspect is also apparent at higher electrolyte concentrations). The reason for these differences is the extent of ionization; in the nonlinear Poisson-Boltzmann equation, the counterions are more tightly associated with the monomers. Note that since the counterions were taken to be pointlike, the

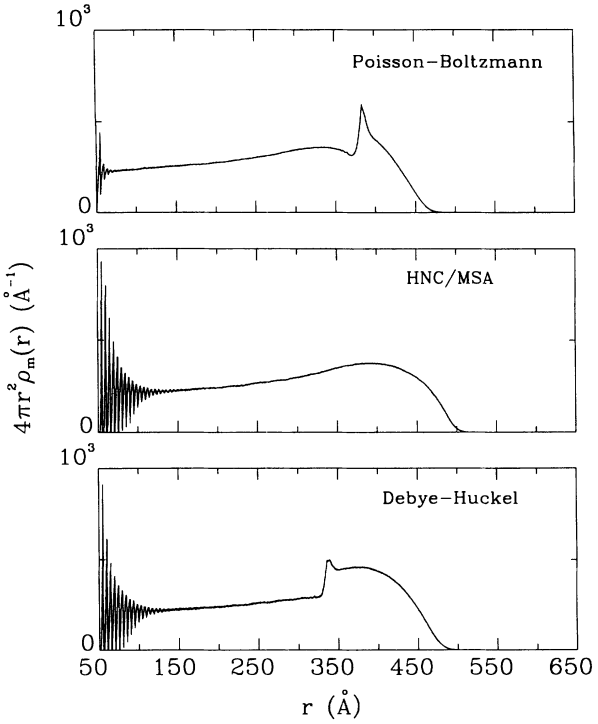

FIG. 15. Monomer density at infinite dilution for case (b) in Table I in a solution where the screening length was 10 Å. The three curves where obtained by using effective monomer potentials, $\phi(r)$, computed within the MSA, cf. Eq. (2.6); within the linearized Debye-Huckel approximation, cf. Ref. [8]; and within the nonlinear Debye-Huckel approximation, cf. Eq. (3.6).

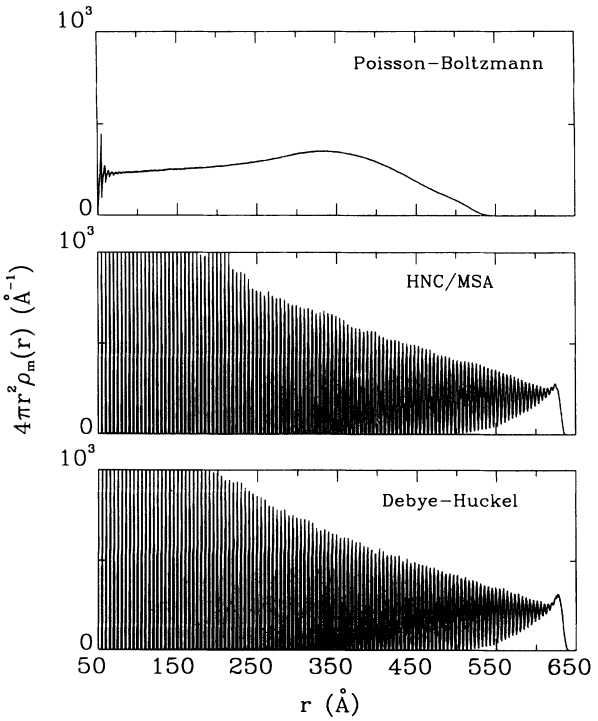

FIG. 16. As in Fig. 15, but for a screening length of 100 Å.

chain will be neutralized to a greater extent than what would be observed if a finite-diameter counterion were used.

As a last example, results showing the dependence on the excluded volume parameter for some longer, neutral chains are shown in Figs. 17 and 18. As expected, increasing the excluded volume leads to a swelling of the polymer layer and, hence, in the effective volume fraction of the suspension. In turn, this leads to an increase in the peak heights seen in the structure factors, a decrease in the compressibility [i.e., $S_{c,c}(k=0)$], and a shift to smaller scattering wave numbers.

The degree of overlap of the polymers attached to different colloids was also examined for neutral chains, and except for very small excluded volume parameters, no significant overlap was observed. The reason for this can be understood in terms of the increase in the number of monomers that interact as the aggregates are forced to overlap. For example, if the polymer layer is modeled as a uniform density spherical shell of outer radius Γ it follows that the aggregate-aggregate excluded volume interaction energy, $u_{c,c}(r)$, becomes

$$\beta u_{c,c}(r) \approx \frac{4\pi}{3}\rho_m^2 \nu(\Gamma - r/2)^2(\Gamma + r/4), \tag{3.8}$$

for $2\Gamma \geq r \geq \Gamma$. For the cases shown in Fig. 17, it easy to show that $\beta u_{c,c}(r)$ quickly becomes much larger than unity as the layers are forced to overlap, and hence, such configurations will not be likely to be observed; charging the polymer can only make matters worse. Of course, this discussion is based on a mean-field picture of the polymer layer; in a very swollen or rodlike state, the spherically symmetric picture of the monomer density may break down. In such cases, if the chains are neutral, it may be possible to intersperse the polymer chains, thereby allowing for more overlap.

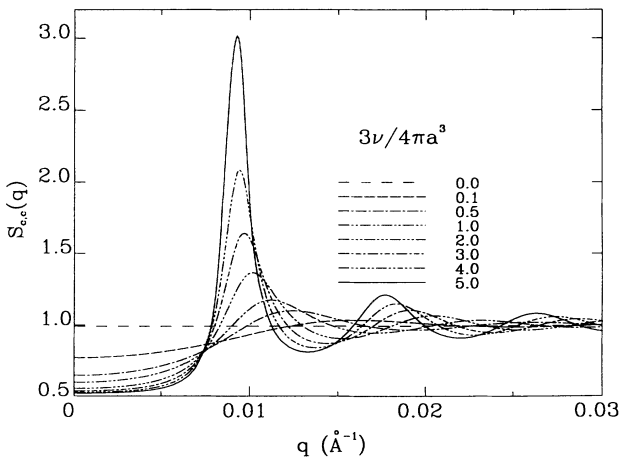

FIG. 17. The effect of increasing the excluded volume interaction on the structure factor for a $3\times10^{-6}M$ suspension composed of colloidal aggregates corresponding to case (c) in Table I.

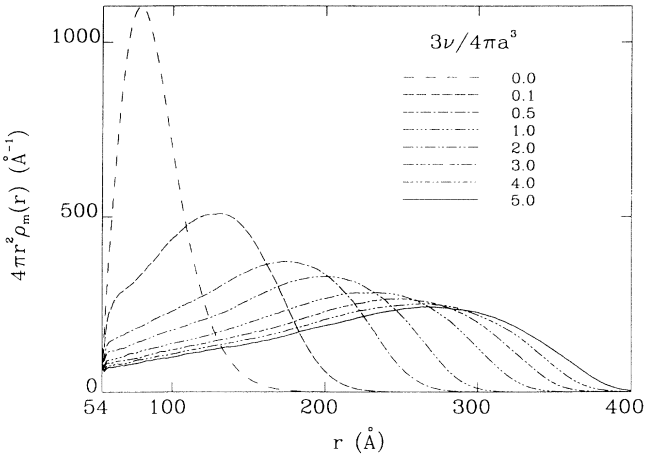

FIG. 18. The effect of increasing the excluded volume interaction on the monomer density for a $3\times10^{-6}M$ suspension composed of colloidal aggregates corresponding to case (c) in Table I.

IV. DISCUSSION

In this work, a numerically tractable theory for the coupled inter- and intra-aggregate equilibria in suspensions of polymer coated colloids has been presented. The approach combines the semianalytic treatment of intra-aggregate pair correlations in systems comprising colloids coated with extended polymer layers, generalized to allow for overlapping layers, with a mean-field Monte Carlo treatment of the average properties of the polymer layers, and a theoretical description of the coupled equilibria has been obtained.

For the examples considered, the results show that increasing the monomer-monomer repulsion, either sterically or Coulombically, leads to a swelling of the aggregate, a concomitant increase in the structural features observed in the aggregate-aggregate pair correlation functions and structure factors, and a rapid decrease in the degree of interpenetration of the polymer layers attached to different colloid cores. This is as expected, and shows that very different results should in general be anticipated in systems where the polymers are attached to freely moving objects instead of fixed, rigid ones (which can force the polymer layers together with energies much greater than k_BT). One aspect of the mean-field approximation may overestimate the effect in situations where neutral chains are nearly fully stretched; i.e., here spherical symmetry has been assumed, in effect distributing the monomers uniformly in solid angle. Should this not be the case, then it is easy to imagine interpenetration taking place by interdigitating the rodlike polymer chains.

The mean-field potentials were constructed in an *ad hoc* manner, and, as was discussed in Sec. II A, this imposes some artificial restrictions on the nature of the microscopic potentials. A more rigorous discussion of the origins of the effective potentials will be presented in the future. The results of the preceding section suggest that the closure used to describe the electrolye is likely to have a profound effect on the degree of ionization of the polymers and, hence, on the configuration of the polymer layer and intra-aggregate correlations. These points will also be investigated in the future, although for other closures it is likely that the analytic simplifications associated with the MSA will probably not be possible and that the finite size of the counterions will have to be considered; both these changes will significantly increase the numerical effort. Finally, note that while the polymer models used here were fairly simplistic, it is trivial to extend the approach to more complicated models, including ones with more realistic bonds between the monomers or more complicated charge distributions.

ACKNOWLEDGMENTS

A portion of this work was supported by the National Sciences and Engineering Research Council of Canada and by Le Fond pour la Formation de Chercheurs et l'Aide à la Recherche du Québec. I thank Diep Nguyen and Adi Eisenberg for many stimulating discussions.

[1] For a recent survey, see, e.g., *Colloid-Polymer Interactions: Particulate, Amphiphilic and Biological Surfaces*, edited by P.L. Dubin and P. Tong, ACS Symposium Series 532 (American Chemical Society, Washington, DC, 1993).

[2] P. Flory, *Principles of Polymer Chemistry* (Cornell University Press, Ithaca, NY, 1971), Chap. XII.

[3] See, e.g., P.G. de Gennes, *Scaling Concepts in Polymer Physics* (Cornell University Press, Ithaca, NY, 1979); K.F. Freed, *Renormalization Group Theory of Macromolecules* (Wiley-Interscience, New York, 1987).

[4] There is a vast literature here. However, see J. P. Valleau, Chem. Phys. **129**, 163 (1989) for an example of simulations of short polyelectrolytes in solution and for a discussion of some of the numerical difficulties involved in the calculation.

[5] K. S. Schweizer and J. G. Curro, Phys. Rev. Lett. **58**, 246 (1987); J. Chem. Phys. **89** 3342 (1988); B.C. Eu and H.H. Gan, *ibid.* **99**, 4084, (1993); **99**, 4103 (1993), and references therein.

[6] D. Ronis, Phys. Rev. A **44**, 3769 (1991).

[7] S. Khan, T. Morton, and D. Ronis, Phys. Rev. A **35**, 4295 (1987).

[8] D. Ronis, Macromolecules **26**, 2016 (1993).

[9] N. Metropolis, A. W. Metropolis, M.N. Rosenbluth, A.H. Teller, and E. Teller, J. Chem. Phys. **21**, 1087 (1953).

[10] The labels indicate the position of the monomer on a polymer chain, the chain, and which colloid the chain is attached to. When necessary, this information will be indicated explicitly.

[11] See, e.g., S. Khan and D. Ronis, Mol. Phys. **60**, 637 (1987).

[12] See, e.g, J. P. Hansen and I. R. McDonald, *Theory of Simple Liquids* (Academic, London, 1976).

[13] L. Belloni, Chem. Phys. **99**, 43 (1985).

[14] See, e.g., E. Y. Sheu, C.-F. Wu, S.-H. Chen, and L. Blum, Phys. Rev. A **32**, 3807 (1985); S.-H. Chen, in *Physics of Amphiphiles: Micelles, Vescicles and Microemulsions*,

Proceedings of the International School of Physics "Enrico Fermi," Course XC, Varenna, Italy, 1983, edited by V. Degiorgio and M. Corti (Elsevier, New York, 1985), p. 281; Y.-S. Chao, E. Y. Sheu, and S.-H. Chen, J. Phys. Chem. **89**, 4862 (1985); D. Bratko, H. L. Friedman, S.-H. Chen, and L. Blum, Phys. Rev. A **34**, 2215 (1986).

[15] Note that the transformation is not unique.

[16] Here the colloids are assumed to be monodisperse. This assumption can easily be relaxed at the expense of more complicated notation, cf. Ref. [6].

[17] However, these modifications must be considered if thermodynamic properties of the system are computed (cf. Ref. [6]).

[18] Note, however, that the electrostatic part of $\Delta u_{p,c}(r)$ will vanish for $r \geq R_{p,c} + L$, where L is the length of a fully stretched polymer.

[19] Here, as in Ref. [8], the polymers are assumed to be isotropically attached to the colloidal cores.

[20] J. P. Hansen and L. Verlet, Phys. Rev. **184**, 150 (1969).

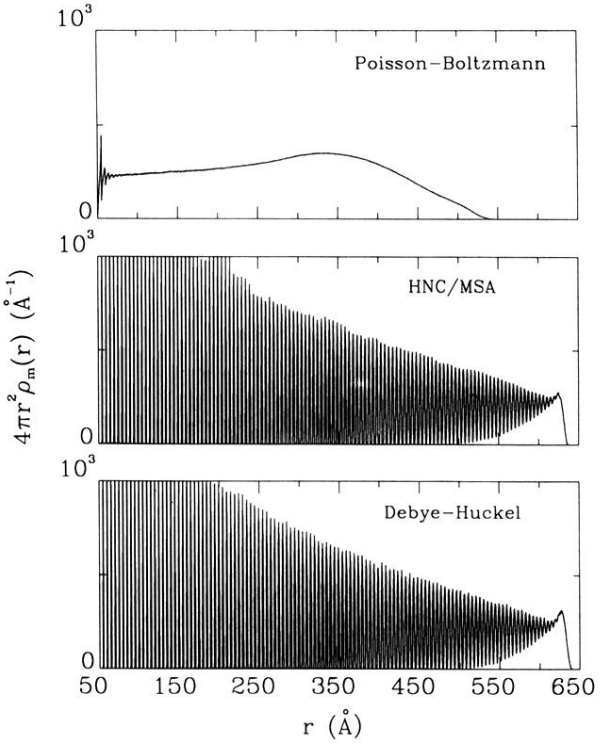

FIG. 16. As in Fig. 15, but for a screening length of 100 Å.